SCIENTIFIC REPORTS

OPEN

SUBJECT AREAS:
FERROELECTRICS AND MULTIFERROICS
CHEMICAL PHYSICS

Received
24 October 2014

Accepted
27 January 2015

Published
27 February 2015

Correspondence and requests for materials should be addressed to J.Z. (jzhu@mail.tsinghua.edu.cn)

Why Sn doping significantly enhances the dielectric properties of $Ba(Ti_{1-x}Sn_x)O_3$

Tao Shi[1], Lin Xie[1], Lin Gu[2] & Jing Zhu[1]

[1]National Center for Electron Microscopy in Beijing, School of Materials Science and Engineering, The State Key Laboratory of New Ceramics and Fine Processing, Laboratory of Advanced Materials, Tsinghua University, Beijing 100084, People's Republic of China, [2]Beijing National Laboratory for Condensed Matter Physics, Institute of Physics, Chinese Academy of Sciences, Beijing 100190, China.

Through appropriate doping, the properties of $BaTiO_3$-based ferroelectrics can be significantly enhanced. To determine the physical process induced by the doping of Sn atoms in $Ba(Ti_{0.8}Sn_{0.2})O_3$, we performed high-resolution scanning transmission electron microscopy experiments and observed that the regions with low Sn content formed polar nano regions (PNRs) embedded in the matrix in $Ba(Ti_{0.8}Sn_{0.2})O_3$. The interactions among Sn, Ti, Ba and O atoms were determined using first principles calculations. Based on the characteristics of the electronic structure and crystal lattice strain fields, the effects of doping with Sn were investigated. The Sn doping not only changed the electronic structure of the crystal but also increased the dielectric properties of the PNRs. Moreover, the Sn doping was also responsible for the diffuse phase transition of the $Ba(Ti_{1-x}Sn_x)O_3$ material. The effects mentioned in this paper are universal in lead-free ferroelectrics, and similar elements such as Sb, Mg, and Zr may have the same functions in other systems. Thus, these results provide guidance for the design of the doping process and new systems of ferroelectric or relaxor materials.

$BaTiO_3$-based ceramics are one of the most studied systems because of their excellent dielectric and electrocaloric[1–2] properties, in addition to their non-toxicity. Because the main origin of the ferroelectricity is hybridisation between B-site atoms and oxygen atoms[3], the basic physical properties of $BaTiO_3$, such as the phase-transition temperatures, lattice constants and permittivity, can be well manipulated via appropriate doping at either the Ti or Ba sites[4]. With the help of a phase diagram, a new type of $BaTiO_3$-based ceramic whose piezoelectric properties are comparable to those of traditional lead-based ferroelectrics was successfully created by introducing Ca and Zr dopants[5]. Specifically, in the $Ba(Ti_{1-x}Sn_x)O_3$ system, the phase is directly determined by the concentration of the Sn element, as determined using the phase diagram[6]. Moreover, as the Sn content is increased, the dielectric permittivity of the ceramics increases to become approximately three times greater than that of pure $BaTiO_3$, and when x is as high as 0.19–0.20, the material transforms from a normal ferroelectric to a typical relaxor ferroelectric[6–7]. In addition to a high dielectric constant, a high electro-caloric effect based on a phase transition has also been reported[8]. Compared with studies about the properties of these materials, there is much less literature about the structure of these materials. One of the main structural features of $Ba(Ti_{1-x}Sn_x)O_3$ ceramics is the diffuse scattering phenomenon in the electron diffraction patterns, which has been suggested to be caused by some nano-size structure[9,10]. Through dark-field and high-resolution transmission electron microscopy images, Xie et al.[11] observed PNRs that were embedded in the matrix in ceramics that exhibited relaxor behaviour. These authors suggested that these PNRs were responsible for both the relaxor behaviour and diffuse scattering phenomenon. In other systems, such as lead-based relaxor ferroelectrics, the effects of the microstructure and lattice dynamics on the relaxor behaviour have been widely reported[12–15]. Recently, in $Ba(Ti_{1-x}Zr_x)O_3$, through first principles and thermodynamic calculations, the relationship between PNRs and chemical distribution along with that between the macroscopic properties and internal electric field have been investigated[16,17,18]. However, in the $Ba(Ti_{1-x}Sn_x)O_3$ relaxor system, an explanation of the microstructure and enormously enhanced dielectric properties remains lacking; thus, understanding how Sn dopants change the structure and why they can strengthen the properties are still critical problems to solve.

In this paper, we investigate the atomic structure and chemical distribution of $Ba(Ti_{0.8}Sn_{0.2})O_3$ using aberration-corrected high-resolution scanning transmission electron microscopy (HRSTEM) and energy-dispersive X-ray spectroscopy (EDS). Based on these experimental results, combined with first principles calculations, the effects of Sn on the electronic structure and crystal lattice strain at the atomic scale are revealed, and a structure

model of the $Ba(Ti_{0.8}Sn_{0.2})O_3$ relaxor is proposed to explain the very strong enhancement of the dielectric permittivity.

Results

An atomic-resolution high-angle annular-dark-field (HAADF) image is shown in Figure 1(a). To more clearly examine the atomic and electric structure, we calculated the displacement of each Ti/Sn column; the results are depicted as yellow arrows in Figures 1(b), (d) and (e), which are enlarged from the red frame in Figure 1(a). These yellow arrows indicate the modulus and direction of the "off-centre" displacements of the Ti/Sn atom columns in each unit cell. To simultaneously see the displacements and chemical distribution more clearly, in Figures 1(d) and 1(e), contour maps are used to show the different values of the displacements and Sn content. It is apparent that in the regions with large displacements, the Sn content is very low. Moreover, in Figure 1(d), the displacements in the red regions are approximately 20 pm, which is significantly larger than the displacements in most of the other regions. Given the additional fact that the size of these red regions is approximately 4–5 unit cells, we considered these regions to be PNRs, which have been widely reported. Therefore, we concluded that the PNRs contained less Sn. The calculations of the displacements and Sn content are provided in Supplemental Information.

This result can also be supported by EDS mapping and annular-bright-field (ABF) experiments. The ABF image, which was acquired at the same time as the HAADF image, is shown in Figure 2(a). Figure 2(b) shows the atomic element mapping of the red frame in Figure 2(a), and this region appears to be one of the PNRs in Figures 1(a) and 1(d) of the HAADF image. The absence of the Sn lattice indicates low Sn content in this area. As a comparison, the mapping of the matrix is shown in Figure 2(c); in this figure, the clear and uniform Sn lattice indicates a much higher concentration. The corresponding spectra for the areas in Figures 2(b) and 2(c) are shown in Figures 2(d) and 2(e), respectively. All of the peaks in the spectra are normalised by the Ba L/Ti K peaks, which are too close to be separated. It is apparent that the Sn Lα peak in Figure 2(e) is much higher than that in Figure 2(d). In detail, the ratio of the Sn Lα line strength and to the Ba L/Ti K line strength is 1 : 5 in Figure 2(e), whereas the value is 1 : 7 in Figure 2(d). The results of the spectra also indicate that the matrix contains more Sn atoms than do the PNRs. Therefore, the EDS and ABF results confirm that the PNRs contain fewer Sn atoms than does the matrix.

Discussion

Our experimental results help to understand the physical behaviour of the Sn in the $Ba(Ti_{1-x}Sn_x)O_3$ system. According to the results of the first principles calculation presented in Figure 3(a), the overlap between Sn and oxygen atoms is significantly less than that between Ti and oxygen atoms, which indicates that the orbital hybridisation between Sn and oxygen atoms is much weaker than that between Ti and oxygen atoms. Because the hybridisation between B-site atoms and oxygen atoms helps to reduce short-range repulsions to allow off-centre ion displacements[3], in normal ferroelectrics, such as $BaTiO_3$, the dipoles caused by off-centre displacements between B-site atoms and the oxygen octahedra can exist in every unit, and the interactions between them are sufficiently strong to form a long-range Coulomb field. This effect directly leads to the domain structure of the crystal, as demonstrated in Figure 3(b). However, in the unit cells in which Sn atoms replace Ti atoms, the dipole can hardly occur. Therefore, in parts of the matrix in which the concentration of Sn atoms is sufficiently high, the continuous dipole-dipole interaction is destroyed, and the long-range Coulomb potential cannot be built up in the matrix, as demonstrated in Figure 3(c). Therefore, the normal ferroelectric domain cannot form; this effect is similar to the phenomenon associated with Mg atoms in $Pb(Nb_{2/3}Mg_{1/3})O_3$[19]. However, the valance of Sn is equal to that of Ti. Consequently, regardless of the lattice configuration, all of the regions can still be charge balanced. Thus, no superstructure exists in the material.

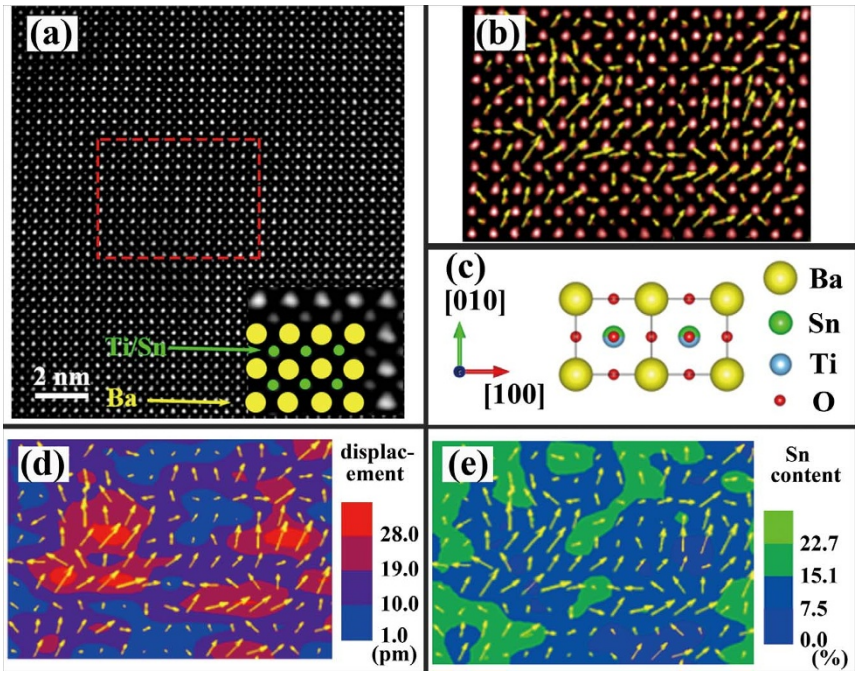

Figure 1 | (a) HAADF image of $Ba(Ti_{0.8}Sn_{0.2})O_3$ viewed from the <001> zone axis. (b) The enlarged images from the red frame in (a); the yellow arrows indicate the displacements of the Ti/Sn column in each unit cell. (c) The projection of the paraelectric phase of $Ba(Ti_{1-x}Sn_x)O_3$ in the <001> crystallographic direction. (d) The displacement distribution map from (b). It is apparent that there are several polar clusters, which are marked in red, and each contains approximately 4 to 5 unit cells. (e) The chemical and displacement distribution map from (b). In the regions in which the arrow is longer, the Sn content, which is represented by the blue areas, is much less. This result indicates that the PNRs contain less Sn than the matrix.

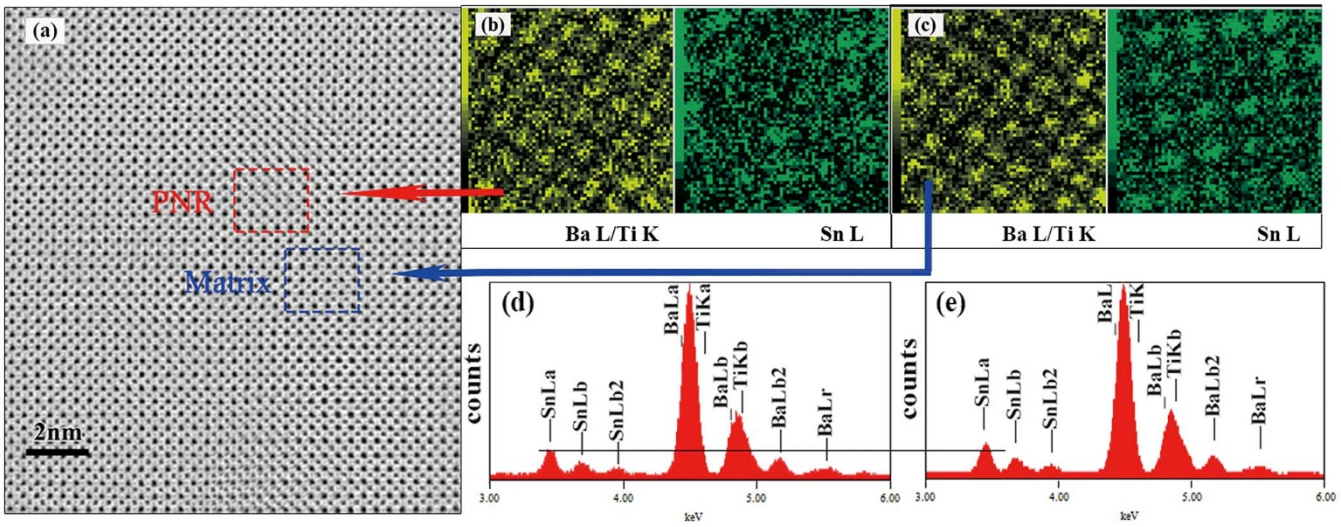

Figure 2 | (a) The ABF image acquired at the same time as the HAADF image shown in Figure 1(a). The area in the red frame is precisely the same location as the polar region shown in Figure 1(b). (b) The chemical element mapping of the region in the red frame in Figure 2(a). The absence of Sn atoms in the element mapping indicates low Sn content in the PNRs. (c) The chemical element mapping of the matrix; the contrast of Sn atoms indicates a high content. Spectra (d) and (e) correspond to Figures 2(b) and 2(c), respectively. All of the peaks in Figures 2(d) and 2(e) are normalised by the peak of Ba L/Ti K. The strength of the Lα peak of Sn atoms is much weaker in Figure 2(d) than that in Figure 2(e), whereas the counts of the Lα peak of Ba atoms are the same in both figures. The ratio of the Lα peaks between Sn atoms and Ba atoms in the PNRs is approximately 1 : 7 and that in the matrix is approximately 1 : 5.

However, in the regions with low Sn content of $Ba(Ti_{1-x}Sn_x)O_3$, the situation is similar to that shown in Figure 3(b). The Coulomb fields exist in these nanometre-size regions and stabilise the polarisation, which explains why the crystal exhibits relaxor behaviour when the Sn content is greater than 0.19–0.20.

However because the radius of the Sn ions (69 pm) is slightly greater than that of the Ti ions (61 pm), according to the close-packing rule of crystals, the lattice constant increases as the concentration of Sn increases; this effect was demonstrated by the XRD experiments (see the Supplemental Information). Therefore, the PNRs, which should possess smaller lattice constants because of their smaller Sn concentration, expand under the stress of the matrix. The stress has a large effect on the ferroelectricity of materials[20]. $BaTiO_3$ thin films on different substrates exhibit different phases, and their dielectric properties are greatly strengthened because of the mismatch strain[20]. When the mismatch strain increases, the coercive force and saturation polarisation increase significantly. In our case, the difference is that the stress on the PNRs is three-dimensional;

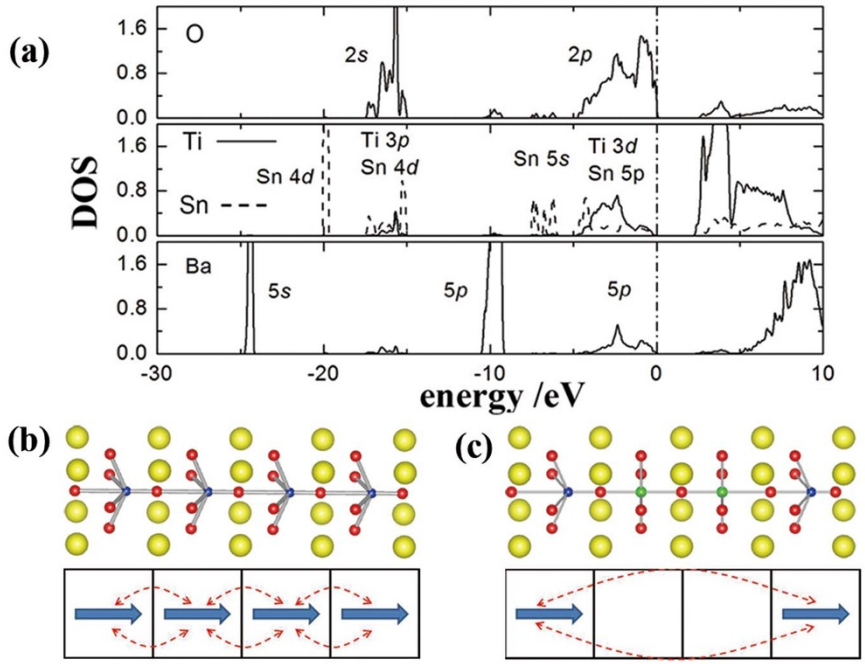

Figure 3 | (a) The partial density of states (DOS) of each element. The DOS of the Sn atom is represented by the dotted line. The energy of the oxygen 2p-state electrons ranges from −4 to 0 eV. In this range, the density of Sn electrons is significantly less than that of Ti electrons, which indicates that the electron orbital hybridisation between Sn and oxygen atoms is much less than that between Ti and oxygen atoms. (b) The interaction of dipoles in the normal ferroelectric material $BaTiO_3$ and the PNRs of $Ba(Ti_{0.8}Sn_{0.2})O_3$. (c) The interaction of dipoles in the matrix of $Ba(Ti_{0.8}Sn_{0.2})O_3$.

however, the effect is similar. Because of the stress, the unit cells of the PNRs expand in three dimensions, which indicates that there is more space between Ti atoms and the oxygen octahedra to allow larger off-centre displacements. Because the off-centre displacement has a direct relationship with the polarisation, the polarisation is strengthened in the PNR; this conclusion can be easily proved using theoretical calculations. Based on the result from the HAADF experiments that the displacements in the PNRs are approximately 20 pm, the polarisation in the PNRs can be calculated according to the equation

$$P = \alpha/V \sim 2ne\Delta r/V, \quad (1)$$

where P represents the local polarisation, n = 4 is the number of effective charges of Ti^{4+} and Sn^{4+}, $\Delta r \sim 20$ pm is the displacement of B-site ions according to the results of the HAADF experiments, and $V \sim (0.404\ nm)^3$ represents the volume of the unit cell (see the Supporting Information). The polarisation in the PNRs is approximately 38.8 $\mu C/cm^2$, whereas the typical remnant polarisation of pure $BaTiO_3$ ceramics is approximately 10 $\mu C/cm^2$. Therefore, the polarisation is truly strengthened in the PNRs.

In addition to these effects, the distribution of the Sn also changes the local Curie temperature in the material. As mentioned above, the Sn destroys the long-range Coulomb potential in the crystal, which indicates that in regions of the matrix with increased Sn concentration, the effect of the Coulomb potential is weak. Therefore, in these regions, the off-centre ion displacements become unstable, which leads to a decrease in the Curie temperature. However, in the regions with less Sn concentration, the dipole-dipole interaction remains sufficiently strong to form PNRs. Nevertheless, the Curie temperature of these areas remains at a higher temperature under the effect of the Coulomb potential. Because the distribution of the Sn element in the material is completely random, the local Curie temperatures also vary; this variation is responsible for the diffuse phase transition behaviour of the $Ba(Ti_{1-x}Sn_x)O_3$ relaxor material.

In summary, using HRSTEM experiments, we have demonstrated that the doping Sn atoms are mainly concentrated outside the PNRs. Based on the electronic structure and crystal lattice strain, which induce the generation of the PNRs and the increase in the polarisation of the PNRs, the role of Sn was determined. Moreover, the local Curie temperature is also related to the concentration of Sn atoms, which directly explains the diffuse phase transition behaviour of $Ba(Ti_{1-x}Sn_x)O_3$. The physical model and mechanism reported here may also apply to other doping systems of $BaTiO_3$-based lead-free relaxors, such as $Ba(Ti_{1-x}Zr_x)O_3$. Consequently, these results may lead to the development of direct relationships among the atomic interactions, structures and relaxor properties of lead-free relaxors. Because our discovery provides a fundamental understanding of the doping element, it can be of benefit for designing the doping process and new systems of ferroelectric and relaxor materials.

Methods

The $Ba(Ti_{0.8}Sn_{0.2})O_3$ ceramics used in this study were prepared using conventional solid-state reactions[7]. The specimens for the electron microscopy experiments were prepared by mechanical grinding and dimpling, followed by ion milling in a stage cooled by liquid nitrogen. The HRSTEM and EDS experiments were performed on an ARM-200F (JEOL, Tokyo, Japan) scanning transmission electron microscope operated at 200 kV with a CEOS Cs corrector (CEOS GmbH, Heidelberg, Germany) to cope with the probe-forming objective spherical abberation, and the HAADF and ABF images were recorded simultaneously. For elemental mapping, the K edge was used for Ti, whereas the L edge was used for Sn and Ba. The first-principles calculations were performed using the VASP software package[21], the plane-wave basis and the PAW scheme[22] with the Perdew-Zunger parameterisation of the exchange-correlation potential[23]. The details of the calculations are described in the Supplemental Material.

1. Moya, X. *et al.* Giant Electrocaloric Strength in Single-Crystal BaTiO3. *Adv. Mater.* **25**, 1360–1365 (2013).
2. Bai, Y. *et al.* Both High Reliability and Giant Electrocaloric Strength in BaTiO3 Ceramics. *Sci. Rep.* **3**, 2895 (2013).
3. Cohen, R. E. Origin of ferroelectricity in perovskite oxides. *Nature* **358**, 136–138 (1992).
4. Shvartsman, V. V. & Lupascu, D. C. Lead-Free Relaxor Ferroelectrics. *J. Am. Ceram. Soc.* **95**, 1–26 (2012).
5. Liu, W. & Ren, X. Large piezoelectric effect in Pb-free ceramics. *Phys. Rev. Lett.* **103**, 257602 (2009).
6. Lei, C., Bokov, A. A. & Ye, Z. G. Ferroelectric to relaxor crossover and dielectric phase diagram in the BaTiO3–BaSnO3 system. *J. Appl. Phys.* **101**, 084105 (2007).
7. Xiaoyong, W., Yujun, F. & Xi, Y. Dielectric relaxation behavior in barium stannate titanate ferroelectric ceramics with diffused phase transition. *Appl. Phys. Lett.* **83**, 2031–2033 (2003).
8. Upadhyay, S. K. *et al.* Electro-caloric effect in lead-free Sn doped BaTiO3 ceramics at room temperature and low applied fields. *Appl. Phys. Lett.* **105**, 112907 (2004).
9. Liu, Y. *et al.* Structured diffuse scattering and polar nano-regions in the $Ba(Ti_{1-x}Sn_x)O_3$ relaxor ferroelectric system. *J. Solid State Chem.* **180**, 858–865 (2007).
10. Liu, Y. & Withers, R. L. Structural disorder, polarisation and the normal to relaxor ferroelectric transition in BaTiO3 based perovskites. *Ferroelectrics* **402**, 3–9 (2010).
11. Xie, L. *et al.* Static and dynamic polar nanoregions in relaxor ferroelectric $Ba(Ti_{1-x}Sn_x)O_3$ system at high temperature. *Phys. Rev. B* **85**, 014118 (2012).
12. Bokov, A. A. & Ye, Z. G. Recent progress in relaxor ferroelectrics with perovskite structure. *J. Mater. Sci.* **41**, 31–52 (2006).
13. Kumar, A. *et al.* In-plane dielectric and magnetoelectric studies of BiFeO3. *Phys. Status Solidi A* **209**, 1207–1212 (2012).
14. Manley, M. E. *et al.* Phonon localization drives polar nanoregions in a relaxor ferroelectric. *Nature Commu.* **5**, 2683 (2014).
15. Bokov, A. A. & Ye, Z. G. Dielectric relaxation in relaxor ferroelectrics. *J. Adv. Dielect.* **2**, 1241010 (2012).
16. Bellaiche, L., García, A. & Vanderbilt, D. Finite-temperature properties of Pb (Zr 1-x Ti x) O 3 alloys from first principles. *Phys. Rev. Lett.* **84**, 5427–5430 (2012).
17. Wang, D. *et al.* Fano resonance and dipolar relaxation in lead-free relaxors. *Nat. Commu.* **5**, 5100 (2014).
18. Pirc, R. & Kutnjak, Z. Electric-field dependent freezing in relaxor ferroelectrics. *Phys. Rev. B* **89**, 184110 (2014).
19. Lu, N. & Zhu, J. Electron low energy-loss functions of Pb $(Mg_{1/3}Nb_{2/3})O_3$: Theory and experiment. *J. Appl. Phys.* **104**, 034109 (2008).
20. Choi, K. J. *et al.* Enhancement of ferroelectricity in strained BaTiO3 thin films. *Science* **306**, 1005–1009 (2004).
21. Kresse, G. & Furthmüller, J. Efficient iterative schemes for ab initio total-energy calculations using a plane-wave basis set. *Phys. Rev. B* **54**, 11169–11186 (1996).
22. Kresse, G. & Joubert, D. From ultrasoft pseudopotentials to the projector augmented-wave method. *Phys. Rev. B* **59**, 1758–1775 (1999).
23. Perdew, J. P. & Zunger, A. Self-interaction correction to density-functional approximations for many-electron systems. *Phys. Rev. B* **23**, 5048–5079 (1981).

Acknowledgments

This work was financially supported by the National 973 Project of China (2015CB654902) and the Chinese National Nature Science Foundation (11374174,51390471). This work made use of the resources of the National Center for Electron Microscopy in Beijing and Tsinghua National Laboratory for Information Science and Technology.

Author contributions

T.S. and J.Z. conceived and designed the experiments. L.G. performed the electron microscopy experiments. L.X. performed the first-principles simulation. T.S. analysed the data. T.S. and J.Z. co-wrote the paper. J.Z. supervised the entire project. All the authors discussed the results and commented on the manuscript.

Additional information

Supplementary information accompanies this paper at http://www.nature.com/scientificreports

Competing financial interests: The authors declare no competing financial interests.

How to cite this article: Shi, T., Xie, L., Gu, L. & Zhu, J. Why Sn doping significantly enhances the dielectric properties of $Ba(Ti_{1-x}Sn_x)O_3$. *Sci. Rep.* **5**, 8606; DOI:10.1038/srep08606 (2015).